

## Hydrophobic collapse and cold denaturation in the Jagla model of water

This article has been downloaded from IOPscience. Please scroll down to see the full text article.

2010 J. Phys.: Condens. Matter 22 284109

(<http://iopscience.iop.org/0953-8984/22/28/284109>)

View [the table of contents for this issue](#), or go to the [journal homepage](#) for more

Download details:

IP Address: 129.98.215.132

The article was downloaded on 22/06/2010 at 14:55

Please note that [terms and conditions apply](#).

# Hydrophobic collapse and cold denaturation in the Jagla model of water

Sergey V Buldyrev<sup>1</sup>, Pradeep Kumar<sup>2</sup>, Srikanth Sastry<sup>3</sup>,  
H Eugene Stanley<sup>4</sup> and Saul Weiner<sup>1</sup>

<sup>1</sup> Department of Physics, Yeshiva University, 500 West 185th Street, New York, NY 10033, USA

<sup>2</sup> Center for Studies in Physics and Biology, University of Texas at Austin, Austin, TX 78712-1167, USA

<sup>3</sup> Jawaharlal Nehru Centre for Advanced Scientific Research, Bangalore 560064, Karnataka, India

<sup>4</sup> Center for Polymer Studies and Department of Physics, Boston University, Boston, MA 02215, USA

Received 11 May 2010

Published 21 June 2010

Online at [stacks.iop.org/JPhysCM/22/284109](http://stacks.iop.org/JPhysCM/22/284109)

## Abstract

The Jagla model is a coarse-grained model of water which describes interactions between groups of water molecules by a spherically symmetric potential characterized by a hard core, a linear repulsive ramp and a long-range attractive ramp. The Jagla model qualitatively reproduces the thermodynamics and dynamics of liquid water including density and diffusion anomalies as well as certain chemical properties such the increase of solubility of small hydrophobic particles upon cooling. We examine, via molecular dynamics simulation, the behavior of the bead-on-a-string polymers of various lengths in the Jagla model. We find that such polymers exhibit swelling upon cooling similar to cold denaturation of proteins in water. We show that while for short polymers the swelling is gradual, longer polymers exhibit a first-order-like phase transition between a globular phase at high temperatures to a random coil state at cold temperatures. This transition is associated with the formation of a liquid–polymer phase boundary surrounding the globule and complete dewetting of the central parts of the globule at high temperatures. We study thermodynamics of this transition and find that the entropy, volume, and potential energy of the solvent–random coil system is lower than those of the globule–solvent system. Accordingly the slope of the coil–globule transition line on a PT plane has positive slope. We present simple thermodynamic considerations similar to classical nucleation theory, which relate the temperature of the cold swelling transition to polymer length and relate the dewetting of the globule to its diameter and to the Egelstaff–Widom length scale.

(Some figures in this article are in colour only in the electronic version)

## 1. Introduction

In addition to its unique properties as a pure liquid [1–4], water is a remarkable solvent [5–28]. Recently it was shown that the Jagla model [29, 30] with a spherically symmetric pair potential (figure 1(a)) reproduces not only the thermodynamic anomalies of pure water, [31–46] (figure 1(b)) but also it reproduces the decrease of solubility of small non-polar compounds with temperature increase as well as the swelling of hydrophobic polymers upon cooling [47]. The latter

phenomenon was interpreted as the basis of cold denaturation of globular proteins [48–51]. The key feature of the Jagla model which allows it to mimic many properties of real water is the existence of the empty space between the particles created by the wide repulsive ramp of the interaction potential [46] (figure 2(a)). In real water the empty space between water molecules is created by the directional four-coordinated hydrogen bonds [52, 53]. This empty space shrinks upon heating, leading to the negative thermal expansion coefficient (density anomaly) as well as to a decrease of solubility of

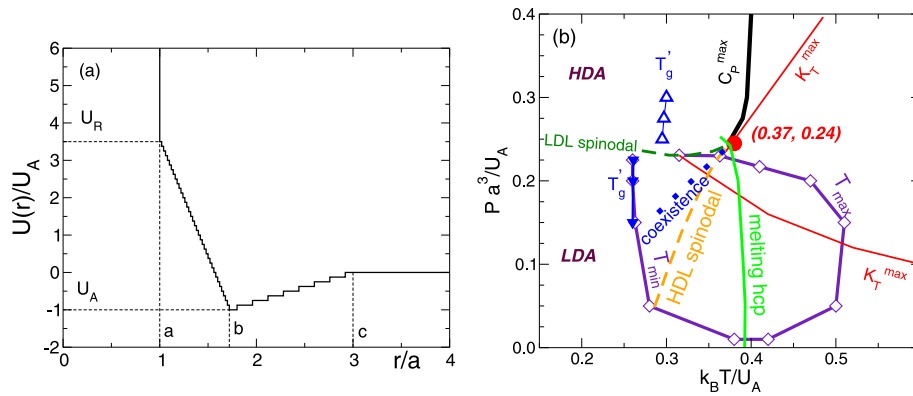


**Figure 1.** (a) The two-ramp spherically symmetric Jagla potential captures much of the ‘two-length scale’ physics corresponding to the first and the second shells in water [44]. The diameter of the hard core  $r_1 = a = 1$  and the diameter of the soft core  $r_2 = b \approx 1.72$  determine the two length scales, corresponding to the first and second shells of water. Small steps are introduced in order to use discrete molecular dynamics [58] (b)  $P$ - $T$  phase diagram of the potential shown in (a). Shown are the liquid–liquid critical point (solid circle), the liquid–liquid coexistence line (dotted line), the lines of maxima of isobaric heat capacity  $C_P^{\max}$  (bold solid line) and isothermal compressibility  $K_T^{\max}$  (thin solid line) as functions of temperature at constant pressure. Near the critical point, these lines merge into the Widom line. Also shown are the loci of temperatures of maximum and minimum density labeled  $T_{\max}$  and  $T_{\min}$  respectively (diamonds), the low density liquid (LDL) and the high density liquid (HDL) spinodals (dashed lines) and the approximate locations of glass transitions  $T'_g$  below which the LDL and HDL become, respectively, low density amorphous (LDA) and high density amorphous solids (triangles). The positions of  $T'_g$  are determined by the positions of the heat capacity maxima caused by restoration of ergodicity upon heating of LDA and HDA [45].

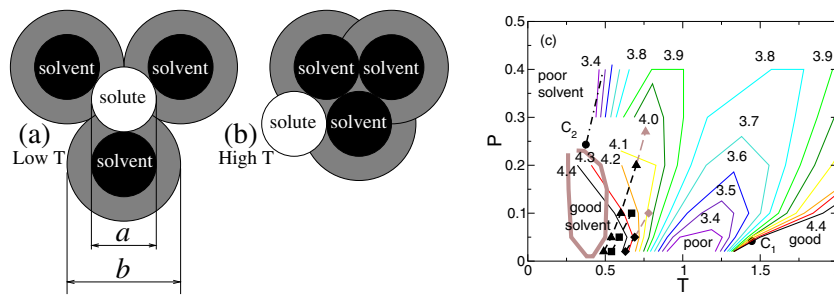


**Figure 2.** (a) and (b) The mechanism of the decrease of solubility of small apolar compounds in the Jagla liquid upon heating. The non-polar compounds are modeled as hard spheres (white circles) of the same diameter  $a$  as the hard core diameter of the Jagla particles (black circles). Gray rims indicate the area of the repulsive ramps of the Jagla particles. (a) At low temperatures, the Jagla particles prefer to stay at the distance  $b$  corresponding to the minimum of the potential in figure 1(a). This configuration has sufficient empty space to fit the non-polar solutes. (b) At higher temperatures, some Jagla particles migrate up the repulsive ramps of their neighbors. This migration simultaneously causes two effects: the increase of the density upon heating (density anomaly) and the decrease of solubility upon heating caused by the reduction of the empty spaces between Jagla particles available to the solutes. (c) The  $P$ - $T$  phase diagram of the Jagla model with lines of equal radius of gyration  $R_g$  of a bead-on-a-string polymer made of  $M = 44$  hard spheres of diameter  $a$  linked by square well bonds with maximal distance  $d = 1.2a$ . The polymer has a minimal radius at low  $P$  in the temperature range between the two critical points of the Jagla model indicated by solid circles (the liquid–gas critical point,  $C_1$  and the liquid–liquid critical point  $C_2$ ). The polymer swells both upon cooling into the density anomaly region (thick gray line) below  $C_2$  and upon heating as the system approaches the liquid–gas coexistence line. At high pressures ( $P \gg P_{c2}$ ) the non-monotonic behavior of  $R_g$  vanishes, giving way to a standard monotonic increase of  $R_g$  upon heating. The polymer collapses as the temperature decreases towards the compressibility maxima line (dash-dot line) emanating from the liquid–liquid critical point. This behavior is related to the fact that HDL is a poor solvent for small apolar solutes [25]. Also shown are the lines of the first-order phase transitions for polymers of lengths  $M = 176$  (triangles),  $M = 132$  (squares) and  $M = 88$  (diamonds). The top gray points for  $M = 176$  and  $M = 88$  are extrapolations for the temperature and pressure at which the step in the system volume, associated with the first-order phase transition, vanishes and the continuous behavior of the thermodynamic state functions is restored.

the small non-polar compounds which at low temperatures can fit between the Jagla particles. In [47] it was found that the gyration radius of small bead-on-a-string polymers dissolved in Jagla liquid has a minimum on the  $P$ - $T$  plane, corresponding to the ambient conditions (figure 2(b)). The polymers swell upon both heating and cooling, and upon pressurizing.

While the radius of gyration of the small polymers changes continuously with temperature, corresponding to the second order phase transition, as expected in the vicinity of the  $\theta$ -point [59–61], the behavior of longer polymers upon cooling into the density anomaly region becomes first-order-like with a characteristic step in  $R_g(T)$  (figure 3) and other thermodynamic state functions such as volume  $V$ , energy

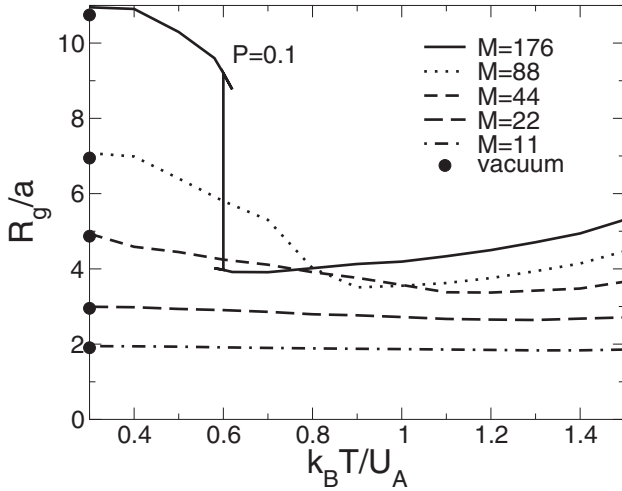


**Figure 3.** Effect of polymer length  $M$  on the swelling behavior at  $P = 0.1$ , below  $P_{c2}$ . While for small  $M \leq 88$  the temperature dependence of  $R_g$  is gradual, consistent with the standard polymer theory, for  $M = 176$  the system exhibits a sharp transition at  $T \approx 0.6$  between the collapsed state with  $R_g \approx 4$  and the swollen state with  $R_g \approx 10$ , corresponding to cold swelling (denaturation). Note that the values of  $R_g$  for  $T \leq 0.5$  for all polymer lengths in the solvent coincide approximately with the values of  $R_g$  of the hard sphere polymer chains of the same length in vacuum (solid circles), indicating that the polymers are in a random coil conformation consistent with dissolution in a ‘good’ solvent.

$U$ , and enthalpy  $H$ . This phenomenon is of key interest in the theory of hydrophobic hydration on large and small scales [7–24]. In this paper we will explore it in detail.

## 2. Methods

The interaction potential  $U(r)$  of the Jagla solvent particles with attractive tail is characterized by five parameters: the hard core diameter  $a$ , the soft core diameter  $b$ , the range of attractive interactions  $c$ , the depth of the attractive ramp  $U_A$  and the height of repulsive ramp  $U_R$  (figure 1) [29]. These parameters can be collapsed into three independent dimensionless ratios:  $b/a$ ,  $c/a$ , and  $U_R/U_A$ . The ratio of the soft core and hard core diameters,  $b/a$ , is a sensitive control parameter that, for the purely repulsive case ( $U_A = 0$ ), determines the fluid’s hard sphere ( $b/a \sim 1$ ) or water-like ( $b/a \sim 7/4$ ) behavior [33]. The latter value of  $b/a$  corresponds closely to the ratio of radial distances from a central water molecule to its second and first-neighbor shells, as measured by the second-nearest and nearest-neighbor peaks of the oxygen–oxygen radial distribution function ( $\approx 4.5$  and  $\approx 2.8$  Å, respectively). Following [29, 42, 43] we select  $b/a = 1.72$ ,  $c/a = 3$ ,  $U_R/U_A = 3.5$ . This choice of parameters produces a phase diagram with several water-like features. It includes two critical points, one corresponding to the first-order liquid–gas transition and the other to a first-order liquid–liquid transition at low temperatures, and a wide region of density anomaly bounded by the locus of temperatures of maximum density (figure 1(b)). The role of the attractive potential,  $b \leq r \leq c$ , is simply to allow fluid–fluid transitions to occur. Water-like

thermodynamic, dynamic and structural anomalies occur even in the purely repulsive case ( $U_A = 0$ ), and their appearance is governed by the ratio  $b/a$  [32].

In this work we adapt a methodology developed in our previous work, the discrete molecular dynamics (DMD) method [54–58]. In order to use the DMD algorithm, we replace the repulsive and attractive ramps with discrete steps (40 and 8, respectively), as described in [42] (see figure 1(a)).

We measure length in units of  $a$ , time in units of  $a(m/U_A)^{1/2}$ , where  $m$  is the particle mass, number density in units of  $a^{-3}$ , pressure in units of  $U_A a^{-3}$ , and temperature in units of  $U_A/k_B$ . This realization of the Jagla model displays a liquid–gas critical point at  $T_{c1} = 1.446$ ,  $P_{c1} = 0.0417$  and  $\rho_{c1} = 0.102$ , and a liquid–liquid critical point at  $T_{c2} = 0.375$ ,  $P_{c2} = 0.243$ ,  $\rho_{c2} = 0.370$  [42]. We model solute particles as hard spheres of diameter  $d_0$ . The hard sphere solutes interact with the Jagla solvent only through excluded volume repulsion, which occurs at the contact distance of  $(a + d_0)/2$ . Here, we choose  $d_0 = a$ , the hard core diameter of the Jagla solvent. The dependence of the solubility on  $d_0$  is an important question that will be addressed in future work.

First we study the behavior of polymers composed of  $M$  monomers modeled by hard spheres of the same diameter as the solute considered above, namely,  $d_0 = a$ . We model covalent bonds by linking the hard spheres with the simplest bond potential

$$U_{\text{bond}}(r) = \begin{cases} \infty & r < d_1 \\ 0 & d_1 < r < d_2 \\ \infty & r > d_2, \end{cases} \quad (1)$$

so that the minimum extent of a bond is  $d_1 = a$  and the maximum extent is  $d_2 = 1.2a$ . We simulate the trajectory of the polymer for  $10^5$  time units at constant  $T$  and  $P$  in a cubic box containing  $N = 4200$  Jagla solvent particles with periodic boundary conditions. We focus on the average polymer radius of gyration  $R_g(T, P)$ , which is indicative of compact versus extended configurations, as well as on other thermodynamic functions such as potential energy  $U$ , volume  $V$ , and enthalpy  $H = U + PV$ . In all our enthalpy calculations we omit the trivial kinetic term  $3/2(N + M)k_B T$ .

In order to relate the behavior of the polymers to the second virial coefficient of the monomers in the framework of the classical Flory theory [59–61], we also compute a potential of mean force  $F(r)$  acting between two monomers separated by a bond described by equation (1), where  $r = (d_1 + d_2)/2$  and  $d_2 - d_1 = \Delta r = 0.1a$ . To find  $F(r)$ , we compute the sum  $\sum \Delta p_r$  of changes of the radial component of the linear momentum of both solute particles due to collisions with all Jagla particles and divide it by the total simulation time:  $F(r) = \sum \Delta p_r / \Delta t$ . In these simulations we first equilibrate the system at constant  $P$  and  $T$  to establish its equilibrium volume  $V(T, P)$  and then perform a production run for constant  $V$  and  $T$ . The simulations are done for  $N = 1000$  Jagla particles and two hard spheres for  $t = 10^4$  time units. We compute the potential of mean force by integrating  $F(r)$  from a sufficiently large cutoff  $r_{\text{max}} = 5a$  to a given

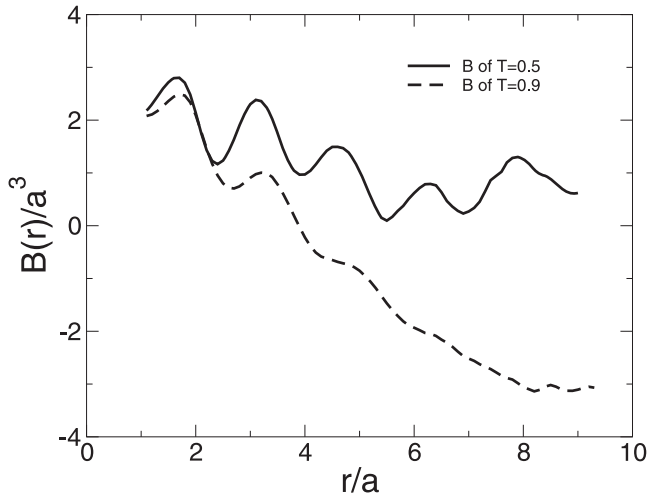


**Figure 4.** Calculation of the second virial coefficient of hard spheres in a Jagla liquid according to equation (3) by integration of the mean force potential at  $P = 0.1U_A/a^3$  for good ( $T = 0.5U_A/k_B$ ) and poor ( $T = 0.9U_A/k_B$ ) solvent conditions. The values of  $B$  are estimated as  $B(r)$  for maximal  $r$ . Large fluctuations of the quantity  $B(r)$ , which are present even at large  $r$ , give a sense of the error bar. Nevertheless one can be confident that for a good solvent the value of  $B$  is positive, while for poor solvent it is negative.

$r < r_{\max}$ :

$$U_{\text{mf}}(r) = U_{\text{mf}}(r_{\max}) + \int_r^{r_{\max}} F(r) dr, \quad (2)$$

where  $U_{\text{mf}}(r_{\max})$  is approximated as the logarithm of the radial distribution function  $U_{\text{mf}}(r_{\max}) = -k_B T \ln[g(r_{\max})]$ . Finally, the second virial coefficient is computed as

$$B(r) = 2\pi/3 \left( a^3 + \int_a^r (1 - \exp(-U_{\text{mf}}(r)/k_B T)) r^2 dr \right). \quad (3)$$

The value of  $B$  is estimated as  $B = \lim_{r \rightarrow \infty} B(r)$ . Figure 4 shows the behavior of  $B(r)$  for  $T = 0.5$  and  $T = 0.9$  at  $P = 0.1$ . We can conclude that for  $T = 0.5$ ,  $B = 0.75 \pm 0.5 > 0$ , indicating good solvent conditions, while for  $T = 0.9$ ,

$B = -3.05 \pm 0.1 < 0$ , indicating poor solvent conditions, in complete agreement with the phase diagram of figure 2(b). A systematic study of the virial coefficient as function of  $T$  and  $P$  will be the subject of our future work.

It is proposed in [60] that in the case of a small third virial coefficient the polymer collapse becomes first-order-like in that the free energy develops a free energy barrier which separates the collapsed and swollen states. Thus it would be interesting to compute the third virial coefficient of hard spheres in the Jagla solvent. However this calculation is very time consuming since it requires integration in three-dimensional space. It is known [60] that the third virial coefficient is small for rigid polymers, which, therefore, undergo a first-order-like collapse transition. Thus an important point in the study of polymer behavior is the analysis of the polymer rigidity and calculation of the conformational entropy of the polymer chain. For polymer conformation, we compute the cosine of the angle between subsequent bonds  $x = \cos(\ell_i \wedge \ell_{i+1})$ , its probability density  $P(x)$  as well as its average  $\langle x \rangle$ , and the conformational entropy  $S_x = -k_B \int_{-1}^1 \ln[P(x)]P(x) dx$  (figure 5). We can see that  $\langle x \rangle$  is very small and never exceeds 0.3. Therefore the studied polymer is very flexible, so it is unlikely that the first-order-like cold swelling transition that we observe is related to the polymer rigidity.

The Egelstaff–Widom length scale [62],  $R_e = \gamma K_T$ , where  $\gamma$  is the gas–liquid surface tension and  $K_T$  is the isothermal compressibility, plays an important role in the theory of hydrophobic hydration at large scales [18]. We find  $\gamma$  from constant volume simulations of the Jagla liquid at a critical density below the gas–liquid critical point  $C_1$  and below the liquid–liquid critical point  $C_2$  in the elongated box  $L_x = L_y \ll L_z$  in which the phases segregate, forming two phase boundaries perpendicular to the  $z$ -axis (figure 6). These phase boundaries pull together the opposite sides of the container perpendicular to the  $x$  and  $y$  axes with forces  $f_x = 2\gamma L_y$  and  $f_y = 2\gamma L_x$ , respectively. These forces decrease the  $P_{xx}$  and  $P_{yy}$  components of the stress tensor relative to the  $P_{zz}$  component unaffected by the surface tension:  $P_{xx} - P_{zz} = -\gamma/L_z$  and  $P_{yy} - P_{zz} = -\gamma/L_z$ . Figure 7 shows the behavior of  $P_{\text{coex}} = P_{zz}$  and  $\gamma$  as function of temperature

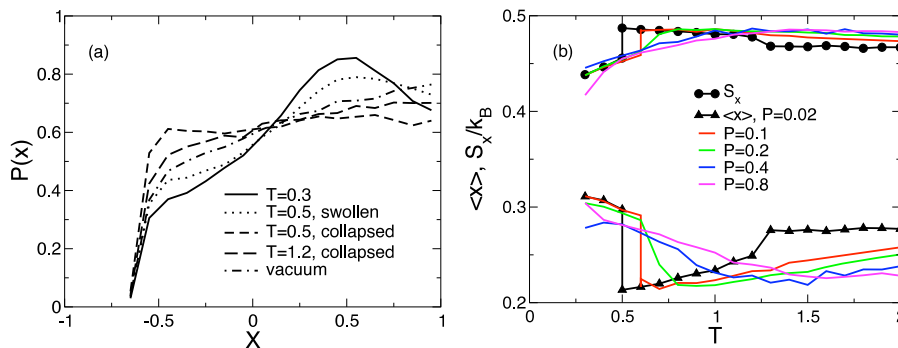


**Figure 5.** Analysis of the polymer backbone geometry for  $M = 176$ . (a) Distribution of bond cosine  $P(x)$  for  $P = 0.02U_A/a^3$ . For a swollen configuration at low  $T$  we can see a distinct peak at  $x = 0.5$ , corresponding to the most probable angle between the bonds of  $60^\circ$ . Obviously this backbone geometry is created by the structure of the solvent. For the collapsed state,  $P(x)$  is almost flat between the largest possible angle ( $x = -0.6$ ) and zero ( $x = 1$ ). (b) Average cosine,  $\langle x \rangle$ , and the conformational entropy,  $S_x$ , as functions of temperature for various pressures. One can see that at the first-order swelling transition line both quantities experience a discontinuous jump, while for large pressures the jump disappears. Interestingly, the conformational entropy of the swollen polymer is lower than that of the collapsed polymer.



**Figure 6.** A snapshot of the pure Jagla liquid phase segregated into HDL and LDL at  $T = 0.33$  below the liquid–liquid critical point  $T_{c2} = 0.374$ . The box size is  $L_x = L_y = L_z/2 = 16.6a$  and the number of atoms is  $N = 3456$ , which corresponds to the density  $\rho = 0.378$ , close to the critical density of the liquid–liquid critical point. While the densities of LDL and HDL are not very different from each other (0.24 and 0.39, respectively) the structure of the liquids are dramatically different. Each HDL particle has on average 3.15 particles within the distance  $1.3a$ , while in LDL this number is 0.54. The pairs of such particles are shown by bonds.

near the gas–liquid and liquid–liquid critical point. Finally, we compute  $K_T$  from the constant pressure simulations of the pure Jagla liquid (figure 8(a)) and multiply it by  $6\gamma$  to obtain the crossover length scale  $6R_e$  at which, according to [18], the crossover from the small scale to the large scale hydrophobic hydration occurs.

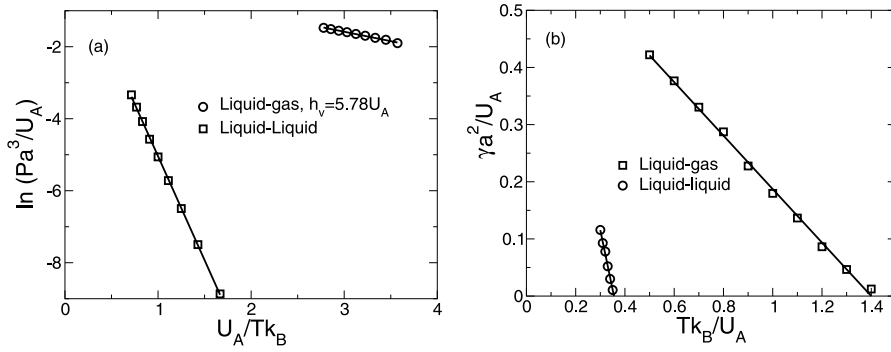
### 3. Results

Figure 3 shows the appearance of the first order phase transition for cold swelling of a sufficiently long polymer. As pressure increases, the temperature of the first-order swelling transition increases and the size of the step in  $R_g(T)$  decreases (figure 9). For pressures above the critical pressure of the liquid–liquid phase transition,  $P > P_{c2}$ , the step disappears and  $R_g(T)$  becomes a continuous function of temperature with a small peak at temperatures above the  $K_T$  maximum on the

$P$ – $T$  phase diagram of the Jagla liquid. As pressure increases further, the peak gets weaker and broader, so that one can expect that at  $P \rightarrow \infty$ ,  $R_g(T)$  becomes a monotonously increasing function of temperature.

To understand the nature of the cold swelling transition we analyze the MD trajectories of the system, measuring  $R_g$ ,  $U$  and  $V$  as function of temperature at constant pressure for sufficiently large polymer length,  $M$ . We characterize energy and volume in terms of the excess quantities of solvation per monomer:  $\Delta u = (U_{JP} - U_J)/M$  and  $\Delta v = (V_{JP} - V_J)/M$ , respectively, where  $U_{JP}$  and  $V_{JP}$  are the potential energy and volume of the system of  $N$  Jagla particles and a polymer of length  $M$  at equilibrium, and  $U_J$  and  $V_J$  are the potential energy and volume of the pure Jagla liquid consisting of the same number of particles,  $N$ , at the same  $T$  and  $P$ . Figure 10 shows the behavior of  $R_g(t)$ ,  $\Delta u(t)$  and  $\Delta v(t)$  at low pressure  $P = 0.02U_A/a^3 < P_{c1}$  at two different temperatures, one below the hypothetical cold swelling transition temperature  $T_s$  ( $T = 0.45U_A/k_B$ ) and another above ( $T = 0.55U_A/k_B$ ). The low temperature trajectory starts from the collapsed initial conformation, while the high temperature trajectory starts from a swollen conformation. One can see that after some time both trajectories undergo a dramatic transition. The swollen conformation collapses (folds) above  $T_s$  and the collapsed conformation swells (unfolds) below  $T_s$ . This behavior is very similar to the behavior of proteins in the vicinity of the cold-denaturation temperature. We ran the simulations for  $t = 10^5 a \sqrt{m/U_A}$  time units, which is equivalent to 76 ns if one uses the values of parameters mapping the Jagla potential to water,  $U_A = 4750 \text{ J mol}^{-1}$ ,  $m = 0.036 \text{ kg mol}^{-1}$ , and  $a = 0.27 \text{ nm}$  [45] for several temperatures in the vicinity of the hypothetical  $T_s$ . The lowest temperature at which we observe folding is  $T = 0.54U_A/k_B$  and the highest temperature at which we observe unfolding is  $T = 0.45U_A/k_B$ . Accordingly we conclude that the folding temperature must be approximately  $T = 0.49 \pm 0.05U_A/k_B$ . One can clearly see that the change in excess volume,  $\Delta \Delta v$ , and energy,  $\Delta \Delta u$ , during swelling are both negative, which means that the cold swelling (denaturation) is an exothermic process. The entropy of the unfolded state is lower than the entropy of the folded state by  $\Delta \Delta s = 0.9k_B$  per monomer. Since the entropy loss due to conformational entropy of a polymer is negligible (about  $0.03k_B$  per monomer, see figure 5), it means that the entropy loss is due to restructuring of solvent around the monomers.

The swelling transition which occurs for  $T = 0.45U_A/k_B$  at  $t = 20000$  takes approximately 500 time units which is negligible compared to the total duration of the simulation. This is consistent with existence of a large free energy barrier separating folded and unfolded states. Figure 10(d) shows the conformations of the polymer during typical unfolding, separated by hundred time units. One can see that the unfolding starts with one of the tails of the polymer penetrating into the liquid while a compact globule creating a cavity in the solvent still exists. This conformation is entropically unfavorable because the solvent around the tail loses a lot of entropy. On the other hand the loss in energy which corresponds to the reduction of the surface energy is still small. In section 5 we



**Figure 7.** (a) Arrhenius plots of the liquid–gas and liquid–liquid coexistence lines. The gas–liquid coexistence line obeys the Arrhenius law  $P(T) = P_0 \exp(h_v/k_B T)$ , with  $h_v = 5.78U_A$  being the enthalpy of vaporization. (b) The behavior of the surface tension in liquid–gas and liquid–liquid phase transitions as a function of temperature obtained from the stress tensor, as described in the text. Both surface tensions vanish in the vicinity of the corresponding critical points, as expected.

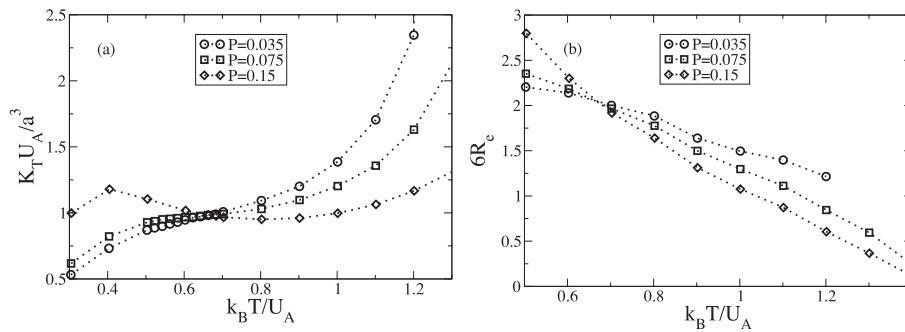


**Figure 8.** (a) Isothermal compressibility as a function of temperature at different pressures. (b) Egelstaff–Widom length scale as a function of temperature computed as a product of isothermal compressibility and surface tension.

will develop a formalism similar to the classical nucleation theory based on this idea. Accordingly, before the polymer successfully unfolds, it makes several unsuccessful attempts, indicated by the spikes in  $R_g(t)$ . Folding of the polymer goes in the reverse way: at first, part of the polymer collapses into a compact globule while the tail of the polymer is still in solvent. In this case the formation of the interface around the collapsed globule costs more energy than the entropy gain of the solvent.

At large pressure, the temperature window around the cold swelling temperature in which no folding or unfolding transitions occur during simulation time shrinks and finally we reach a regime in which many folding–unfolding transitions can be observed for the same trajectory if the temperature is kept near the cold swelling transition (figure 11).

We collect the histograms of  $R_g$ ,  $\Delta u$  and  $\Delta v$ . for several temperatures near the cold swelling transition,  $T_s = 0.69U_A/a^3$ ,  $P = 0.20$  (figure 12). All the distributions become clearly bimodal in the vicinity of  $T_s = 0.69U_A/a^3$ . One peak corresponds to the folded state, another to the unfolded state. Now  $T_s$  can be precisely determined as the temperature at which the areas under both peaks are equal to each other. One can also detect the maxima of the peaks and thus determine  $R_g$ ,  $\Delta u$ , and  $\Delta v$  of the folded and unfolded states at coexistence. At higher pressures, the two peaks merge and the first-order phase cold swelling transition gives way to a gradual transition like in the vicinity of the critical point.

To characterize the thermodynamics of the polymer hydration we compute the excess thermodynamic parameters  $\Delta u$  and  $\Delta v$  for a wide range of temperatures, several polymer lengths, and several pressures (figure 13). One can see that both excess potential energy and volume for large enough  $M$  have a discontinuous jump at low temperatures corresponding to the cold swelling. The temperature of the transition increases as  $M$  decreases and size of the jump decreases. For large  $P$  and small  $M$ , the jump disappears, and the transition becomes continuous, as one can see for  $P = 0.1$  and  $M = 88$ .

For the swollen conformations, the excess volume and energy does not depend on  $M$ , which would be the case for solvation of isolated monomers. For the collapsed state the excess energy per monomer increases when  $M$  decreases. This clearly indicates that the energy jump is caused by the formation of the liquid interface around the polymer globule because the surface area scales as  $M^{2/3} < M$ . For the volume we have the opposite effect, which indicates that the larger the polymer size the more complete is the dewetting of the interior of the globule. Note that for large enough temperatures the effect changes its sign again. This is consistent with the fact that at large temperatures dewetting is not complete.

The graphs also indicate that both excess energy and volume decrease with the increase of pressure, with one notable exception: the excess volume increases with pressure for the cold-swollen polymer. This is consistent with the solvation scheme illustrated in figure 2(a). This picture is

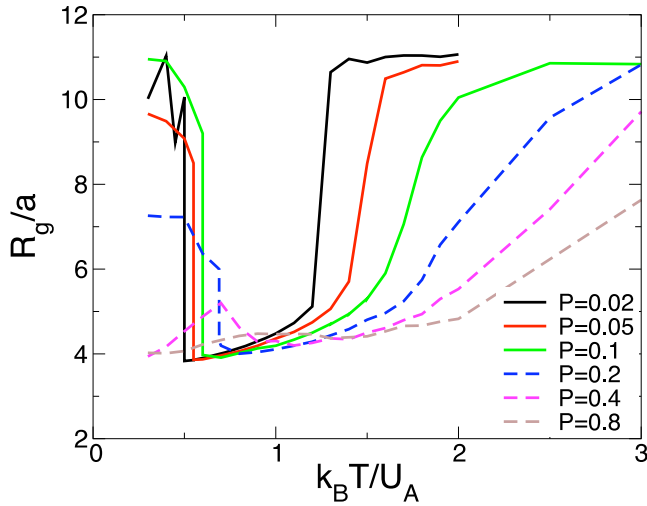


**Figure 9.** Behavior of the radius of gyration,  $R_g$ , of a long polymer ( $M = 176$ ) as a function of temperature at different pressures. Below the liquid–liquid critical point ( $P < P_{c2}$ ), cold swelling has features of the first-order phase transition, with an abrupt change of the collapsed globular conformation of a protein to a random coil conformation upon cooling, with both states existing in some temperature range around the transition point for a sufficiently long time to be investigated. At higher pressures the size of the jump in  $R_g$  becomes smaller and eventually the cold swelling transition completely disappears.

also consistent with the fact that the excess energy for cold-swelled polymer becomes negative at large pressures. Indeed at large pressures in the absence of monomers, more Jagla particles would climb the repulsive ramp, which would lead to an increase in energy and a decrease in volume.

Another prominent feature of the graphs are the huge peaks in  $\Delta u$  and  $\Delta v$  at large  $T$  in the regions of large compressibility caused by the gas–liquid critical point. Large compressibility implies large density fluctuations, the presence of which makes it easier for the polymer to produce large voids in the structure of the liquid.

We measure the sizes of jumps in  $\Delta \Delta u$  and  $\Delta \Delta v$  as a function of cold swelling transition temperature  $T_s$ , which varies with pressure (figure 14). We also find the change in enthalpy  $\Delta \Delta h = \Delta \Delta u + P \Delta \Delta v$  and entropy  $\Delta \Delta s = \Delta \Delta h / T_s$ . Since both entropy and volume decrease for the cold swelling transition, the slope of the cold swelling transition line  $dP/dT = \Delta \Delta s / \Delta \Delta v$  must be positive. This implies that polymers must unfold upon pressurizing at constant temperature. Numerical integration of  $dP/dT$  gives consistent results with the graph  $T_s(P)$  obtained by locating the cold swelling transition temperature from the jumps in  $\Delta u$ ,  $\Delta v$  and the behavior of  $R_g$ . The positive slope of the cold swelling transition line implies that, at small temperatures, the polymer swells upon pressurizing [25]. This phenomenon corresponds to pressure denaturation of proteins.

#### 4. Density profiles and Egelstaff–Widom length scale

The central paradigm of the large scale hydration theory [8, 15] is the formation of the solvent interface around a large

hydrophobic object. Originally it was proposed that the surface of such an object undergoes complete dewetting manifested in the formation of a vapor-like layer of reduced density. However, later it became clear [22] that no noticeable reduction of the density of the liquid near the hydrophobic objects can be observed, instead, what increase around such an object are density fluctuations. The polymer globule is not a hard sphere, it is porous and hence the solvent can penetrate inside it. Here we will show that the first-order-like cold swelling is associated with complete dewetting of the globule interior and the formation of the polymer–liquid interface around the polymer globule. The standard Flory–Huggens–de Gennes theory of polymer collapse implies that the polymer interaction with solvent can be modeled by introducing an effective attractive potential between the monomers. However, if the collapsed polymer globule is completely free of solvent, this is no longer a true assumption. Accordingly we will present simplified considerations which describe this cold swelling transition in terms of the surface tension of the liquid around the globule, much as in classical nucleation theory (section 5). As a first step towards such a theory, we will show that the collapsed globule is indeed encapsulated into an approximately spherical phase boundary, with no solvent molecules inside it. Figure 15 shows the average density profiles of monomers (Hs) and Jagla particles as functions of the distance from the center of mass of the polymer for several different temperatures. At low pressure  $P = 0.02U_A/a^3 < P_{c1}$ , large polymers undergo a sharp cold swelling transition at  $T = T_s = 0.49U_A/k_B$  (figure 9). Here we present two density profiles for collapsed and swelled states collected at  $T = 0.5U_A/K_B$  for  $10^5$  time units during which no folding or unfolding transition occurs.

For the swollen state the density of monomers is very low in the center and gradually decreases outwards; the density of solvent near the center has practically no reduction. In the collapsed state, the density of monomers stays approximately constant in the center of the globule,  $\rho_0 = 0.435/a^3$ , which corresponds to the volume per particle  $v_0 = 2.3a^3$ . The solvent does not penetrate inside the radius  $r_g = 0.29a$ . These profiles strongly suggest the existence of a well-defined polymer–solvent interface. However there is no significant reduction of the total density near the globule, indicating the absence of a vapor-like layer around the globule. The radius of the completely dewetted globule  $r_g$  is significantly larger than  $6R_e = 2.2a$  that can be estimated from figure 8(b). As can be seen from figure 9 at  $P < P_{c1}$ ,  $R_g$  exhibits another sharp swelling transition near the liquid–gas coexistence line at  $T = 1.23U_A/K_B$  (figure 7(a)). Just below the coexistence line the equilibrium vapor density is  $0.014/a^3$ , so one can see that some vapor of density  $0.006/a^3$  is present in the region of the dewetted globule. The density of the monomers in the globule significantly decreases compared to  $T = 0.5U_A/k_B$  and the decay of polymer concentration becomes much more gradual outside the globule. However the radius of the dewetted globule is still the same as at low temperature.

Also, one can see a decrease of the overall particle density near the globule. This decrease may indicate formation of a vapor-like layer around the globule. Interestingly, at  $T = 1.3U_A/K_B$ , above the coexistence line, this vapor

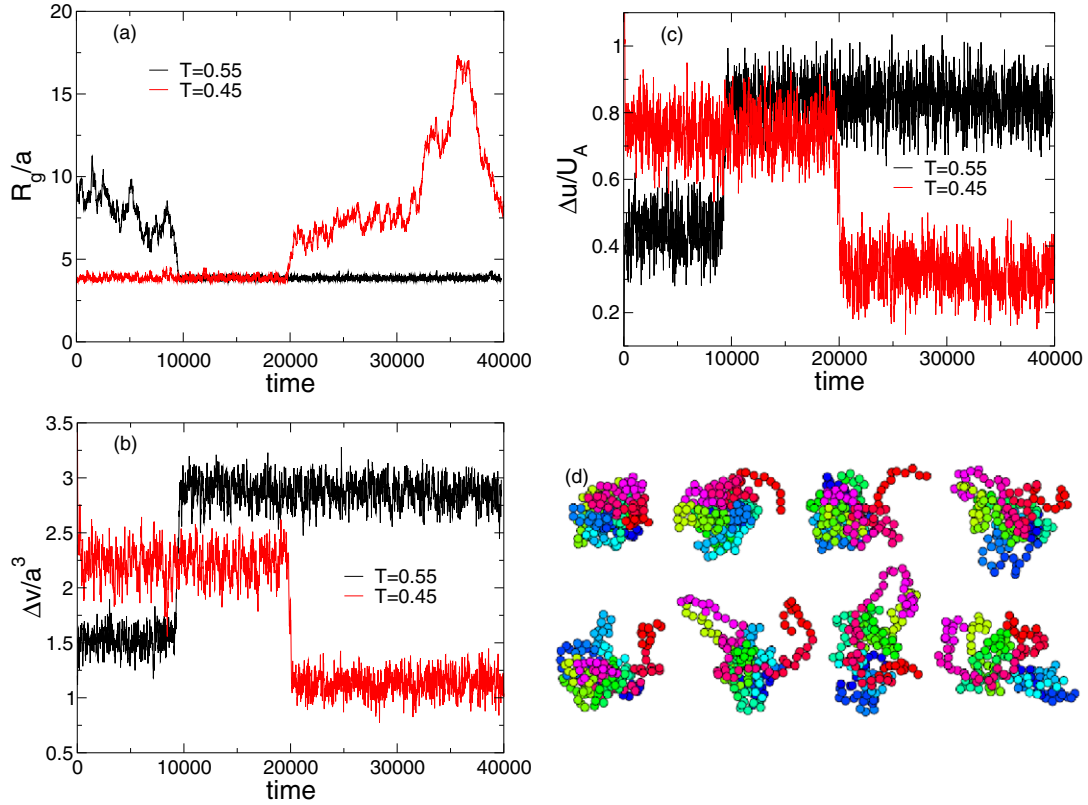


**Figure 10.** (a) Behavior of the radius of gyration of a long polymer ( $M = 176$ ) as a function of time during collapse ( $T = 0.55U_A/k_B$ ) and swelling ( $T = 0.45U_A/k_B$ ) near the temperature of cold swelling,  $T_s = 0.49U_A/k_B$ , at  $P = 0.02U_A/a^3$ . Behavior of energy (b) and volume (c) for the same trajectories as in (a). (d) The snapshots of the polymer conformation near the unfolding transition. The time interval between the snapshots is 100 time units  $a\sqrt{m/U_A}$ . The direction of time corresponds to the first row from left to right and then to the second row from left to right.

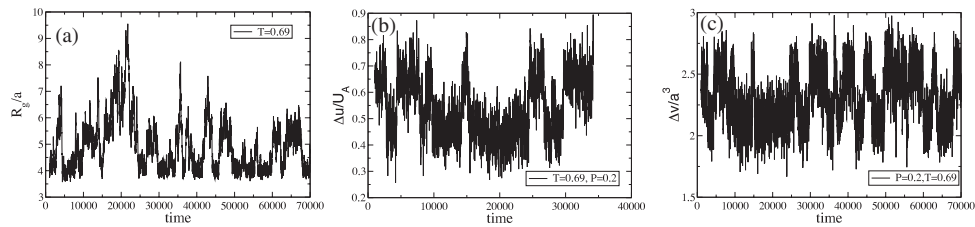


**Figure 11.** (a) Behavior of the radius of gyration of the long polymer ( $M = 176$ ) as a function of time at the cold swelling transition temperature  $T_s = 0.69U_A/k_B$  corresponding to constant pressure simulations  $P = 0.2U_A/a^3$ . Behavior of energy (b) and volume (c) for the same trajectory as in (a).

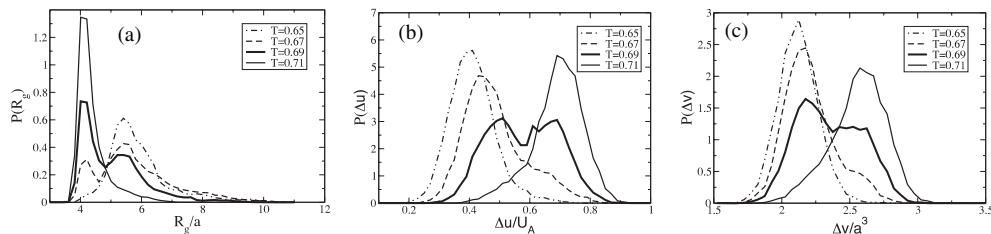


**Figure 12.** Probability density functions of the thermodynamic parameters of the system at  $T_s = 0.69U_A/k_B$  corresponding to constant pressure simulations at  $P = 0.2U_A/a^3$ : (a) radius of gyration, (b) excess potential energy, (c) excess volume.

bubble serves as a nucleus of the vapor phase. Thus, in the simulation started at this temperature from a compact globule conformation, the liquid surrounding the globule after some

initial period of metastability completely vaporizes, the volume dramatically increases and the polymer completely unfolds. In contrast, in the simulation of the pure Jagla liquid at  $T = 1.3$

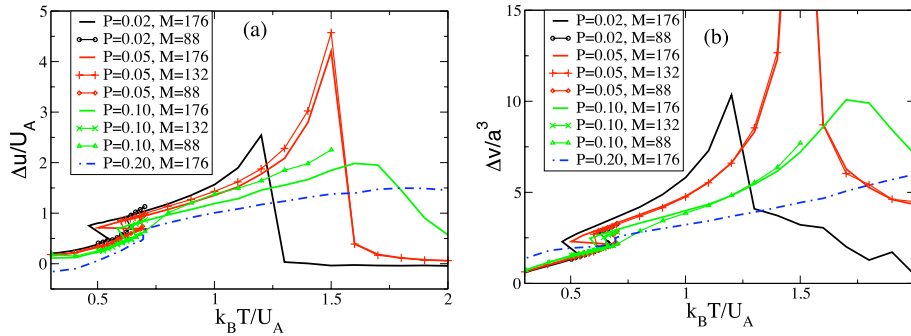


**Figure 13.** Behavior of the excess potential energy (a) and the excess volume (b) per monomer as functions of temperature for different polymer lengths ( $M = 176, 132, 88$ ) and different pressures, ( $P = 0.02, 0.05, 0.1, 0.2U_A/a^3$ ). The z-shape jumps in the graphs indicate the first-order cold swelling transitions. Cold swelling is associated with both decrease in volume and energy, and hence with negative enthalpy. The peaks in the graphs at large temperature are caused by the crossing of the system of either a liquid–gas coexistence line at  $P = 0.02U_A/a^3 < P_{c1}$ , or the Widom line associated with the gas–liquid critical point for  $P > P_{c1}$ , near which the fluid properties rapidly change from liquid-like to gas-like. In the dilute gaseous phase, as  $T \rightarrow \infty$  at constant pressure,  $\Delta u$  and  $\Delta v$  must both converge to zero.

or the liquid surrounding a short polymer of length  $M = 44$ , around which no vapor is formed (figure 16), the liquid remains metastable for the entire duration of the simulation. Thus our results suggest that the vapor-like layer may indeed exist around large hydrophobic objects in the vicinity of the liquid–gas phase transition line.

For larger pressure,  $P = 0.2U_A/a^3$  (figure 15(b)), near the end of the first-order cold swelling transition line at low temperatures ( $T = 0.3U_A/k_B$ ) in the domain of the density anomaly in the LDL phase, the polymer is still completely expanded, however its density near the center is approximately two times larger than at  $P = 0.02U_A/a^3$ , which is consistent with much smaller  $R_g$  values in the swollen state at  $P = 0.2U_A/a^3$  than at  $P = 0.02U_A/a^3$ , as can be seen in figure 9.

Above the cold swelling transition at  $T = 0.8U_A/k_B$ , the density profiles are very similar to those for  $P = 0.02U_A/a^3$  at  $T = 0.5U_A/k_B$  for the collapsed state. The density of monomers in the center of the globule is exactly the same as for lower pressure, but the radius of complete dewetting,  $r_g \approx 2.0a$ , decreases and becomes comparable to  $6R_e$ , which at these conditions is  $\approx 1.9a$ . This is consistent with the fact that we are at the end of the first-order cold swelling transition line above which dewetting can occur, because the Egelstaff–Widom length scale,  $6R_e$  can be regarded as the minimal radius of the hydrophobic sphere near which the phase boundary of the liquid can be formed. At  $T = 0.7U_A/k_B$ , the polymer constantly folds and unfolds (figure 11), so the density profiles collected over the entire simulation represent average densities for folded and unfolded states.

For high pressures,  $P = 0.4U_A/a^3 > P_{c2}$ , (figure 15(c)), the first-order cold swelling transition completely disappears, however  $R_g$  retains its non-monotonous character with a maximum at  $T = 0.7U_A/k_B$  and a minimum at  $T = 1.1U_A/k_B$ . At very small temperatures ( $T = 0.3U_A/k_B$ ) in the domain of HDL, the polymer remains in the collapsed state and its density near the center is the same as in the collapsed state at low pressures, but this state is not associated with dewetting and the density of Jagla particles inside the globule remains high. At the temperature of maximal  $R_g$ , the density of the polymer decreases, and the density of the Jagla particles

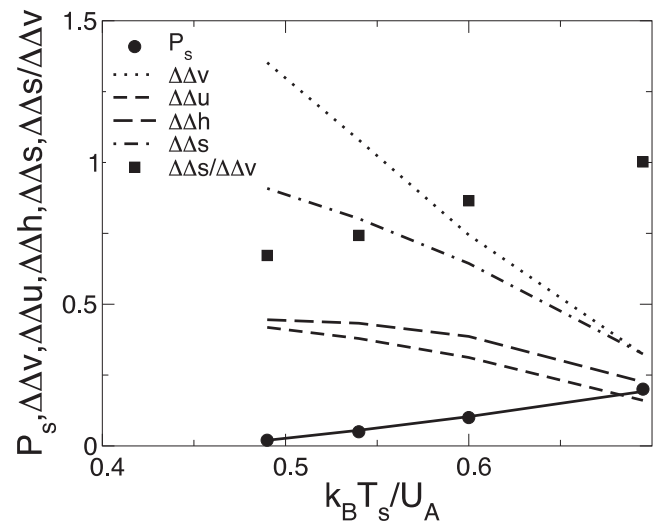


**Figure 14.** Changes of the excess thermodynamic properties at the cold swelling first-order phase transition line  $P_s(T_s)$ : potential energy  $\Delta\Delta u$  (dashed line), volume  $\Delta\Delta v$  (dotted line), enthalpy  $\Delta\Delta h = \Delta\Delta u + P\Delta\Delta v$  (long dashed line), entropy  $\Delta\Delta s = \Delta\Delta h/T_s$  (dash-dotted line) computed for a polymer of length  $M = 176$ . We also compute the slope of the  $P_s(T_s)$  line using the Clapeyron equation as  $\Delta\Delta s/\Delta\Delta v$  (squares) and compare the integral of this slope (solid line) with the directly measured  $P_s(T_s)$  (circles).

near its center does not decrease. At the temperature of the minimum  $R_g$ , the density of the polymer increases again, and the density of solvent decreases dramatically near its center and vanishes at  $r_g \approx 0.5a$ , however this value is less than  $6R_e$ . Thus, no well-defined liquid interface is formed around the globule, and the first-order cold swelling transition disappears. At very high pressure,  $P = 0.8U_A/a^3$  (figure 15(d)), the polymer density remains almost the same in the entire range of temperatures from  $T = 0.3U_A/k_B$  to  $T = 1.5U_A/k_B$ , and the density of solvent remains high near its center, which is consistent with complete disappearance of cold swelling.

To further test the significance of the Egelstaff–Widom length scale we study the density profiles for shorter polymers, in the cases where the first-order cold swelling can still be

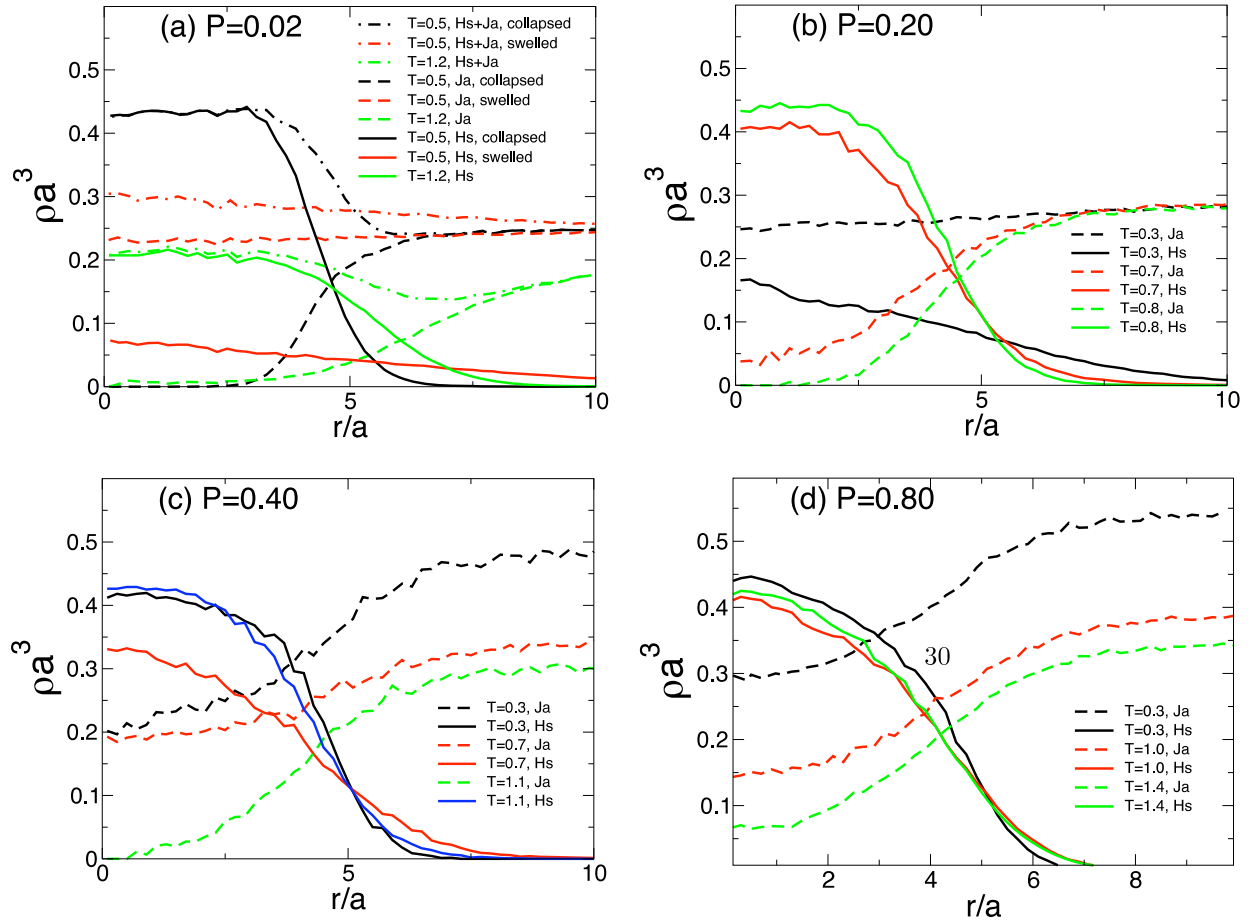


**Figure 15.** Density of hard sphere monomers (Hs, solid lines) and Jagla particles (Ja, dashed lines) as functions of the distance  $r$  from the center of mass of the polymer of length  $M = 176$  at various pressures. (a) The lowest pressure  $P = 0.02U_A/a^3 < P_{c1}$ . Here we also show the total density of particles (dot-dashed lines). (b) Intermediate pressure,  $P = 0.2U_A/a^3 < P_{c2}$ , at which the first-order cold swelling transition still exists, (c) high pressure,  $P = 0.4U_A/a^3 > P_{c2}$ , at which cold swelling still takes place but becomes continuous. (d) Very high pressure, at which cold swelling completely disappears.

observed and when it completely disappears (figure 16). We show the density profile for the polymer of  $M = 88$  at  $P = 0.02U_A/a^3$ ,  $T = 0.7U_A/k_B > T_s$ . At  $T = T_s = 0.63U_A/k_B$ , the polymer constantly folds and unfolds, but the density distribution of volume and energy retains its bimodal character, thus the first-order cold swelling transition is still present. The density of the monomer near the center of the polymer ( $\rho_0 = 0.41/a^3$ ) is only slightly smaller than the density of polymer of  $M = 176$  at similar conditions. However, the region of complete dewetting shrinks ( $R_g \approx 1.8$ ) and become comparable to  $6R_e \approx 1.8$  at the same conditions. For  $P = 0.1U_A/a^3$  the polymer of  $M = 88$  unfolds gradually upon cooling, which is consistent with the absence of dewetting in the center of the globule even at  $T = 0.84U_A/k_B$ , the temperature of the minimal  $R_g$ . A smaller polymer of  $M = 44$  unfolds gradually even at  $P = 0.02U_A/a^3$ , accordingly no complete dewetting of its center is observed. Moreover, this polymer can exist inside the metastable liquid at  $T = 1.3U_A/k_B$ , and does not produce a nucleus of the vapor phase as the polymer of length  $M = 176$  does at the same conditions. This is also consistent with the absence of the liquid interface around this polymer.

### 5. Snake-hatching model of the cold swelling transition

Here we present simplified quantitative considerations which may explain the first-order nature of the cold swelling transition. As we can see from the snapshots of figure 10(d), the unfolding starts with one tail of the polymer trying to penetrate the solvent through the phase boundary, much as a snake hatches from an egg. We assume that the enthalpy change in the cold swelling transition  $\Delta\Delta h$  is largely associated with the formation of the phase boundary, which scaled with the polymer length as  $M^{2/3}$ . If this is true the change in energy per monomer in the cold swelling transition must decrease with  $M$  as  $M^{-1/3}$ . This indeed can be seen from the graphs in figure 13(b), where one can see that for  $T > T_s$  the energy of solvation per monomer  $\Delta u$  for  $M = 88$  goes above the energy for  $M = 188$ , while for  $T < T_s$  these values coincide. Since  $\Delta\Delta h < 0$  the entropy of the swollen state must be smaller than the entropy of the collapsed state. The only explanation of this is that the solvent around the solvated tail of the polymer has less entropy, because monomers occupy the free spaces between the solvent

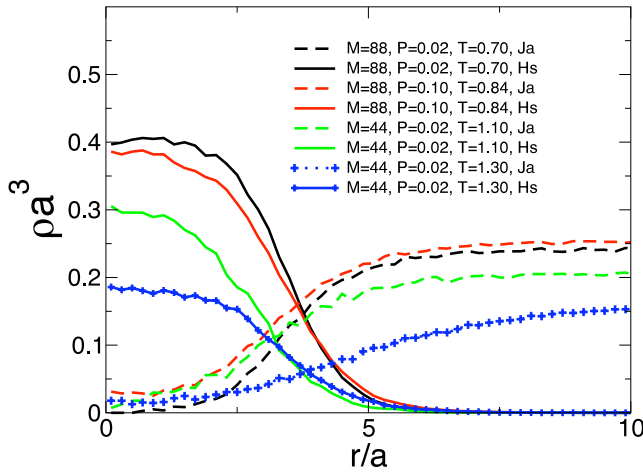


**Figure 16.** Disappearance of complete dewetting for short polymers of  $M = 88$  and  $44$  shown by the density profiles of hard sphere monomers (Hs, solid lines) and Jagla particles (Ja, dashed lines) as functions of the distance  $r$  from the center of mass of the polymer for different  $T$  and  $P$ .

particles, restricting the number of possible configurations available for the solvent particles. This reduction of the entropy obviously is proportional to the length of solvated tail of the polymer  $M_s$ . The value of this entropy  $s_0 < 0$  per monomer must be of the order of magnitude of  $\Delta\Delta s$ . We neglect the entropy of the polymer chain in the solvent and in the globule. In this approximation, the excess Gibbs potential of the system is

$$\Delta G = 4\pi r_g^2 \gamma - T s_0 M_s, \quad (4)$$

where  $\gamma$  is surface tension and  $r_g$  is the radius of the globule, which can be found from the number of monomers remaining in the globule  $M_g = M - M_s$  from the equation  $4\pi r_g^3/3 = M_g/\rho_0$ , where  $\rho_0$  is the density of the monomers in the globule. Finally, we can write

$$\Delta G(y) = G_0[(1 - y)^{2/3} + ay], \quad (5)$$

where  $y = M_s/M$  is the fraction of the monomers in the dissolved state and  $G_0 = \Delta G(0)$  is the Gibbs potential of the collapsed state:

$$G_0 = \gamma(36\pi M^2/\rho_0^2)^{1/3}, \quad (6)$$

and

$$a = -T s_0 (M\rho_0^2/36\pi)^{1/3}/\gamma > 0. \quad (7)$$

Figure 17 shows the behavior of  $\Delta G(y)$  as function of  $y$  for several different temperatures close to  $T_s$ . The fully collapsed state corresponds to  $y = 0$ , the fully swollen state corresponds to  $y = 1$ . The two states are separated by the free energy barrier corresponding to the maximum of the Gibbs potential. The condition of equilibrium  $T = T_s$  corresponds to equal Gibbs potentials of these states:  $\Delta G(0) = \Delta G(1)$ , from where  $a = 1$  and

$$T_s = -\gamma(M\rho_0^2/36\pi)^{-1/3}/s_0. \quad (8)$$

We can see that  $T_s$  decreases with polymer size as  $M^{-1/3}$ , which agrees very well with our numerical results (figure 2(c)).

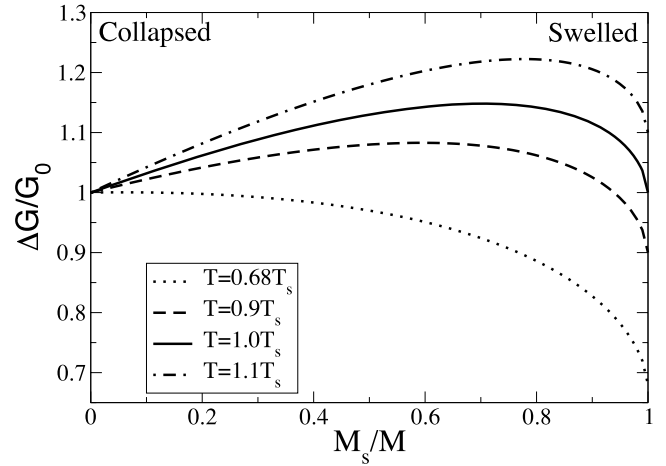


**Figure 17.** Normalized Gibbs potential,  $\Delta G/G_0$ , as a function of the fraction of monomers,  $y = M_s/M$ , in the solvated part of the polymer in the hatching snake model for several different temperatures near the cold swelling temperature,  $T_s$ . At  $T = T_s$  (bold line) the Gibbs potential of swollen and collapsed states are equal to  $G_0$ .

Moreover, if we use  $\rho_0 = 0.43$ ,  $\gamma = 0.42$ ,  $M = 176$ ,  $s_0 = \Delta\Delta s = -0.9$ , we get  $T_s = 0.7$ , which is not very far away from reality, given the crudeness of our approximations. Moreover, equation (5) predicts the correct behavior of the stability of the swollen and collapsed states with temperature, and also the increase in the Gibbs potential energy barrier  $4/27G_0$  separating the two states at equilibrium with the length of the polymer. To demonstrate the increase of  $T_s$  with pressure using equation (8) we need to know the behavior of  $s_0$  and  $\gamma$  with pressure; this will be the subject of future studies.

## Acknowledgments

This paper is a contribution that concerns recent progresses in the field of computer simulations of water discussed at the CECAM workshop ‘Modeling and Simulation of Water at Interfaces from Ambient to Supercooled Conditions’ supported by ESF-Simbioma and CECAM.

We thank C A Angell, S Garde, A Yu Grosberg, D Chandler, and Z Yan for helpful discussions, and the NSF Collaborative Research in Chemistry Program for financial support (CHE0404699, CHE0404695, CHE0404673). We are grateful to P G Debenedetti and P Rossky for their important contributions at the early stages of this project and for their continuous encouragement of this research. SVB acknowledges the partial support of this research through the Dr Bernard W Gamson Computational Science Center at Yeshiva College.

## References

- [1] Franks F 2000 *Water: A Matrix for Life* 2nd edn (Cambridge: Royal Society of Chemistry)
- [2] Eisenberg D and Kauzmann W 1969 *The Structure and Properties of Water* (New York: Oxford University Press)
- [3] Debenedetti P G 2003 *J. Phys.: Condens. Matter* **15** R1669–726

- [4] DeBenedetti P G and Stanley H E 2003 *Phys. Today* **56** (6) 40–6
- [5] Tanford C 1980 *The Hydrophobic Effect: Formation of Micelles and Biological Membranes* 2nd edn (New York: Wiley)
- [6] Kauzmann W 1959 *Adv. Protein Chem.* **14** 1–63
- [7] Ashbaugh H S, Truskett T M and DeBenedetti P G 2002 *J. Chem. Phys.* **116** 2907–21
- [8] Stillinger F H 1973 *J. Solution Chem.* **1** 141–58
- [9] Pratt L R and Chandler D 1977 *J. Chem. Phys.* **67** 3683–704
- [10] Dill K A 1990 *Biochemistry* **29** 7133–55
- [11] Garde S, Hummer G, Garcia A E, Paulaitis M E and Pratt L R 1996 *Phys. Rev. Lett.* **77** 4966–8
- [12] Hummer G, Garde S, Garcia A E, Pohorille A and Pratt L R 1996 *Proc. Natl Acad. Sci. USA* **93** 8951–5
- [13] Hummer G, Garde S, Garcia A E, Paulaitis M E and Pratt L R 1998 *Proc. Natl Acad. Sci. USA* **95** 1552–5
- [14] Hummer G, Garde S, Garcia A E, Paulaitis M E and Pratt L R 1998 *J. Phys. Chem. B* **102** 10469–82
- [15] Lum K, Chandler D and Weeks J 1999 *J. Phys. Chem. B* **103** 4570–7
- [16] Ashbaugh H S, Garde S, Hummer G, Kaler E W and Paulaitis M E 1999 *Biophys. J.* **77** 645–54
- [17] Pratt L R 2002 *Annu. Rev. Phys. Chem.* **53** 409–36
- [18] Rajamani S, Truskett T M and Garde S 2005 *Proc. Natl Acad. Sci. USA* **102** 9475–80
- [19] Ashbaugh H S and Pratt L R 2006 *Rev. Mod. Phys.* **78** 159–78
- [20] Athawale M V, Goel G, Ghosh T, Truskett T M and Garde S 2007 *Proc. Natl Acad. Sci. USA* **104** 733–8
- [21] Widom B, Bhimalapuram P and Koga K 2003 *Phys. Chem. Chem. Phys.* **5** 3085–93
- [22] Godawat R, Jamadagni S N and Garde S 2009 Characterizing hydrophobicity of interfaces using cavity formation, solute binding, and water correlations *Proc. Natl Acad. Sci. USA* **106** 15119–24
- [23] Sarupria S and Garde S 2009 Quantifying water density fluctuations and compressibility of hydration shells of hydrophobic solutes and proteins *Phys. Rev. Lett.* **103** 037803
- [24] Goel G, Athawale M V, Garde S and Truskett T M 2008 Attractions, water structure, and thermodynamics of hydrophobic polymer collapse *J. Phys. Chem. B* **112** 13193–6
- [25] Paschek D 2005 *Phys. Rev. Lett.* **94** 217802
- [26] Paschek D, Nonn S and Geiger A 2005 *Phys. Chem. Chem. Phys.* **7** 2780–6
- [27] Garde S, Garcia A E, Pratt L R and Hummer G 1999 *Biophys. Chem.* **78** 21–32
- [28] Errington J R, Boulougouris G C, Economou I G, Panagiotopoulos A Z and Theodorou D N 1998 *J. Phys. Chem. B* **102** 8865–73
- [29] Jagla E A 1998 *Phys. Rev. E* **58** 1478–86
- [30] Jagla E A 1999 *J. Chem. Phys.* **111** 8980–6
- [31] Kumar P, Buldyrev S V, Sciortino F, Zaccarelli E and Stanley H E 2005 *Phys. Rev. E* **72** 021501
- [32] Yan Z, Buldyrev S V, Giovambattista N and Stanley H E 2005 *Phys. Rev. Lett.* **95** 130604
- [33] Yan Z, Buldyrev S V, Giovambattista N, DeBenedetti P G and Stanley H E 2006 *Phys. Rev. E* **73** 051204
- [34] Head-Gordon T and Stillinger F H 1993 *J. Chem. Phys.* **98** 3313–27
- [35] Garde S and Ashbaugh H S 2001 *J. Chem. Phys.* **115** 977–82
- [36] Hemmer P C and Stell G 1970 *Phys. Rev. Lett.* **24** 1284–7
- [37] Kincaid J M and Stell G 1977 *J. Chem. Phys.* **67** 420–9
- [38] Stillinger F H and Stillinger D K 1997 *Physica A* **244** 358–69
- [39] Sadr-Lahijany M R, Scala A, Buldyrev S V and Stanley H E 1998 *Phys. Rev. Lett.* **81** 4895–8
- [40] DeBenedetti P G, Raghavan V S and Borick S S 1991 *J. Phys. Chem.* **95** 4540–51
- [41] Buldyrev S V, Franzese G, Giovambattista N, Malescio G, Sadr-Lahijany M R, Scala A, Skibinsky A and Stanley H E 2002 *Physica A* **304** 23–42
- [42] Xu L, Buldyrev S V, Angell C A and Stanley H E 2006 *Phys. Rev. E* **74** 031108
- [43] Xu L, Kumar P, Buldyrev S V, Chen S H, Poole P H, Sciortino F and Stanley H E 2005 *Proc. Natl Acad. Sci. USA* **102** 16558–62
- [44] Yan Z, Buldyrev S V, Kumar P, Giovambattista N, DeBenedetti P G and Stanley H E 2007 *Phys. Rev. E* **76** 051201
- [45] Xu L, Buldyrev S V, Giovambattista N, Angell C A and Stanley H E 2009 Monatomic system with a liquid–liquid critical point and two distinct glassy states *J. Chem. Phys.* **130** 054505
- [46] Buldyrev S V, Malescio G, Angell C A, Giovambattista N, Prestipino S, Saija F, Stanley H E and Xu L 2009 Unusual phase behavior of one-component systems with two-scale isotropic interactions *J. Phys.: Condens. Matter* **21** 504106
- [47] Buldyrev S V, Kumar P, DeBenedetti P G, Rossy P J and Stanley H E 2007 Water-like solvation thermodynamics in a spherically symmetric solvent model with two characteristic lengths *Proc. Natl Acad. Sci.* **104** 20177–82
- [48] Privalov P L and Gill S J 1988 *Adv. Protein Chem.* **39** 191–234
- [49] Privalov P L 1990 *Crit. Rev. Biochem. Mol. Biol.* **25** 281–305
- [50] Tsai C-J, Maizel J V Jr and Nussinov R 2002 *Crit. Rev. Biochem. Mol. Biol.* **37** 55–69
- [51] Marqués M I, Borreguero J M, Stanley H E and Dokholyan N V 2003 *Phys. Rev. Lett.* **91** 138103
- [52] Poole P H, Sciortino F, Grande T, Stanley H E and Angell C A 1994 *Phys. Rev. Lett.* **73** 1632–5
- [53] Truskett T M, DeBenedetti P G, Sastry S and Torquato S 1999 *J. Chem. Phys.* **111** 2647–56
- [54] Frenkel D and Smit B 1996 *Understanding Molecular Simulation: From Algorithms to Applications* (San Diego, CA: Academic)
- [55] Rapaport D C 1997 *The Art of Molecular Dynamics Simulation* (Cambridge: Cambridge University Press)
- [56] Alder B J and Wainwright T E 1959 *J. Chem. Phys.* **31** 459–66
- [57] Rapaport D C 1978 *J. Phys. A: Math. Gen.* **11** L213–7
- [58] Buldyrev S V 2008 Application of discrete molecular dynamics to protein folding and aggregation *Aspects of Physical Biology (Series: Lecture Notes in Physics)* ed G Franzese and M Rubi (Berlin: Springer) pp 97–132
- [59] Flory P J, Orwoll R A and Virj A 1964 *J. Am. Chem. Soc.* **86** 3507–14
- [60] Grosberg A Y and Khokhlov A R 1997 *Giant Molecules* (London: Academic)
- [61] Rubinstein M and Colby R H 2003 *Polymer Physics* (Oxford: Oxford University Press)
- [62] Egelstaff P A and Widom B 1970 *J. Chem. Phys.* **53** 2667–9